ACS APPLIED MATERIALS & INTERFACES

Research Article

www.acsami.org

Superhydrophobic Surface with Hierarchical Architecture and Bimetallic Composition for Enhanced Antibacterial Activity

Mei Zhang,[†] Ping Wang,[‡] Hongyan Sun,*[,‡] and Zuankai Wang*[,†]

[†]Department of Mechanical and Biomedical Engineering and [‡]Department of Biology and Chemistry, City University of Hong Kong, Hong Kong, China

ABSTRACT: Developing robust antibacterial materials is of importance for a wide range of applications such as in biomedical engineering, environment, and water treatment. Herein we report the development of a novel superhydrophobic surface featured with hierarchical architecture and bimetallic composition that exhibits enhanced antibacterial activity. The surface is created using a facile galvanic replacement reaction followed by a simple thermal oxidation process. Interestingly, we show that the surface's superhydrophobic property naturally allows for a minimal bacterial adhesion in the dry environment, and also can be deactivated in the wet solution to enable the release of biocidal agents. In particular, we demonstrate that the higher solubility nature of the thermal oxides created in the thermal oxidation process, together with the synergistic cooperation of bimetallic composition and hierarchical architecture, allows for the release of metal ions in a sustained and accelerated manner, leading to enhanced antibacterial performance in the wet condition as well. We envision that the ease of fabrication, the versatile functionalities, and the robustness of our surface will make it appealing for broad applications.

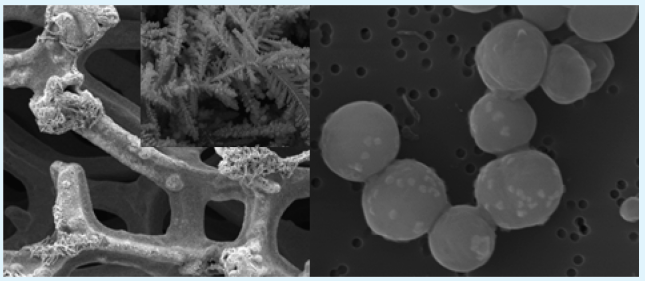

KEYWORDS: *antibacterial, superhydrophobic, bimetallic, hierarchical*

1. INTRODUCTION

Engineering robust artificial biomaterials that can resist bacterial colonization and biofilm formation is of importance for a wide range of applications such as in marine, petroleum pipelines, textiles, and medical implants, yet has proved challenging.[1−5] Antibacterial agents such as antibiotics have been extensively used to protect the public health in our daily life. However, the growing concern about antibiotic resistance has made it imperative to engineer more effective antimicrobial therapies. In particular, there is a renewed interest in developing efficient metal-based antibacterial agents due to their broad-spectrum antibacterial performances and relatively lower toxicity to human cells.[6−9] Although silver has been used as an antimicrobial since antiquity, the specific mechanism of action remains elusive. Recently, studies have shown that silver ion can bind the biological thiol groups in enzymes,[10,11] generate reactive oxygen species (ROS),[12−15] and disrupt the bacterial respiratory chain.[16,17]

Since the adhesion of bacteria to the substrate represents the first step in the bacterial colonization and subsequent biofilm formation,[18−20] the creation of novel surfaces that prevent the initial attachment of bacteria to the substrate emerges as an appealing alternative to a traditional chemical-based approach.[1] Many natural surfaces, including plant leaves, gecko foot, shark skin, insect wings, fish scale, and spider silk, are capable of resisting bacterial colonization.[21−25] Inspired by these natural surfaces, numerous superhydrophobic surfaces[26−33] have been extensively developed over the past decade. Although artificial superhydrophobic surfaces[34−36] can maintain antifouling in the dry conditions for a long time, the desired antifouling property is prone to being compromised in the wet environment due to the breakdown of their water repellency.[31,37−40]

Here, we report a novel superhydrophobic surface with hierarchical architecture and bimetallic composition (Cu/Ag) that exhibits superior antibacterial activity under various working conditions. The surface is fabricated through a facile galvanic replacement approach[41−44] followed by a simple thermal oxidation process. Remarkably, we show that the metal oxides created by the thermal oxidation process facilitate the antifouling property in the dry condition due to its low surface energy and also can be dissolved for the release of metal ions in water. Moreover, the higher solubility nature of these thermal oxides,[45−49] together with the synergistic cooperation of bimetallic composition and hierarchical architecture, enables the release of metal ions in a sustained and accelerated manner, leading to enhanced antibacterial activity in the wet condition as well.

2. EXPERIMENTAL SECTION

Sample Preparation. The hierarchical bimetallic composite surface was fabricated using a simple galvanic exchange process. Briefly, the porous copper foam substrate was first cleaned by ultrasonic treatment in ethanol, followed by washing with 1 M

Received: August 15, 2014
Accepted: November 24, 2014
Published: November 24, 2014

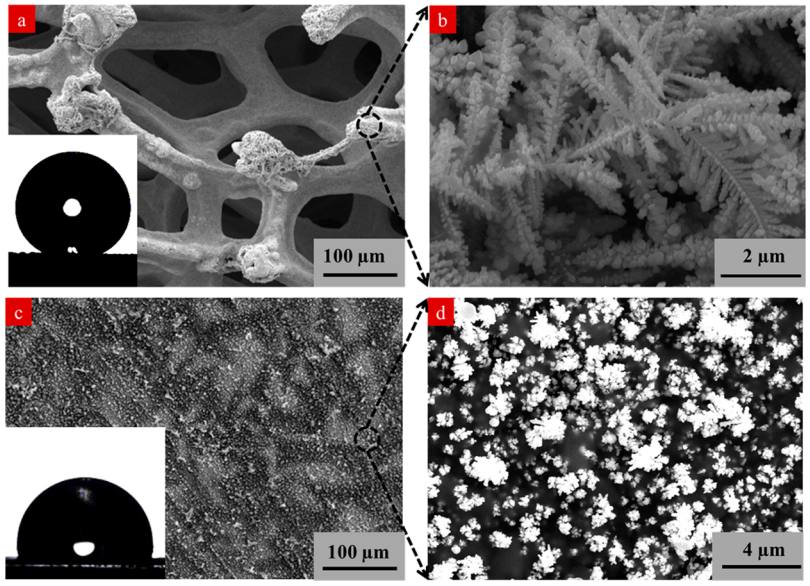

Figure 1. Scanning electron microscope (SEM) images of as-fabricated hierarchical Ag/Cu composite and nanostructured Ag/Cu composite. (a) SEM image showing that the hierarchical bimetallic composite is covered by dense silver dendrites. The contact angle of bacterial suspension on the surface is 158.59° (inset). (b) The silver dendrites are composed of nanoparticles 100 ± 20 nm in diameter. The length and width of silver dendrites are 8 ± 0.8 μm and 2.5 ± 0.7 μm, respectively. (c) SEM image of the nanostructured bimetallic composite fabricated on the flat copper foil. The contact angle of bacterial suspension on the surface is 111.16° (inset). (d) Silver nanostructures are in a coral-like shape, with an average length of 4 ± 1 μm and width of 0.8 ± 0.2 μm.

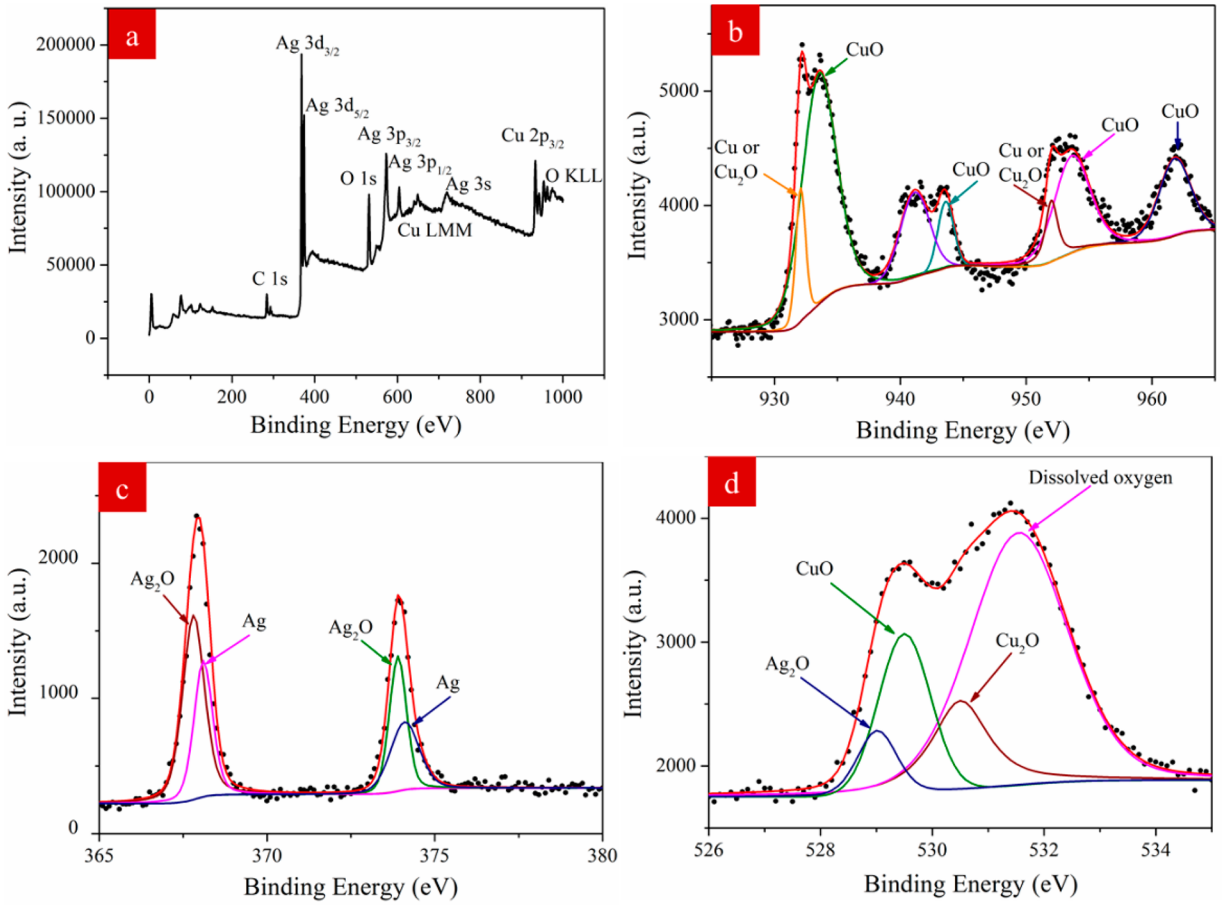

Figure 2. XPS spectra analysis. (a) The characteristic peaks corresponding to the hierarchical bimetallic composite at 530.5 (O 1s) and 974.8 eV (O KLL) result from the dissolved oxygen or the thermal oxidation of copper and silver in the heating stage. (b–d) High-resolution XPS spectra analysis showing the chemical states of Cu, Ag, and O, respectively.

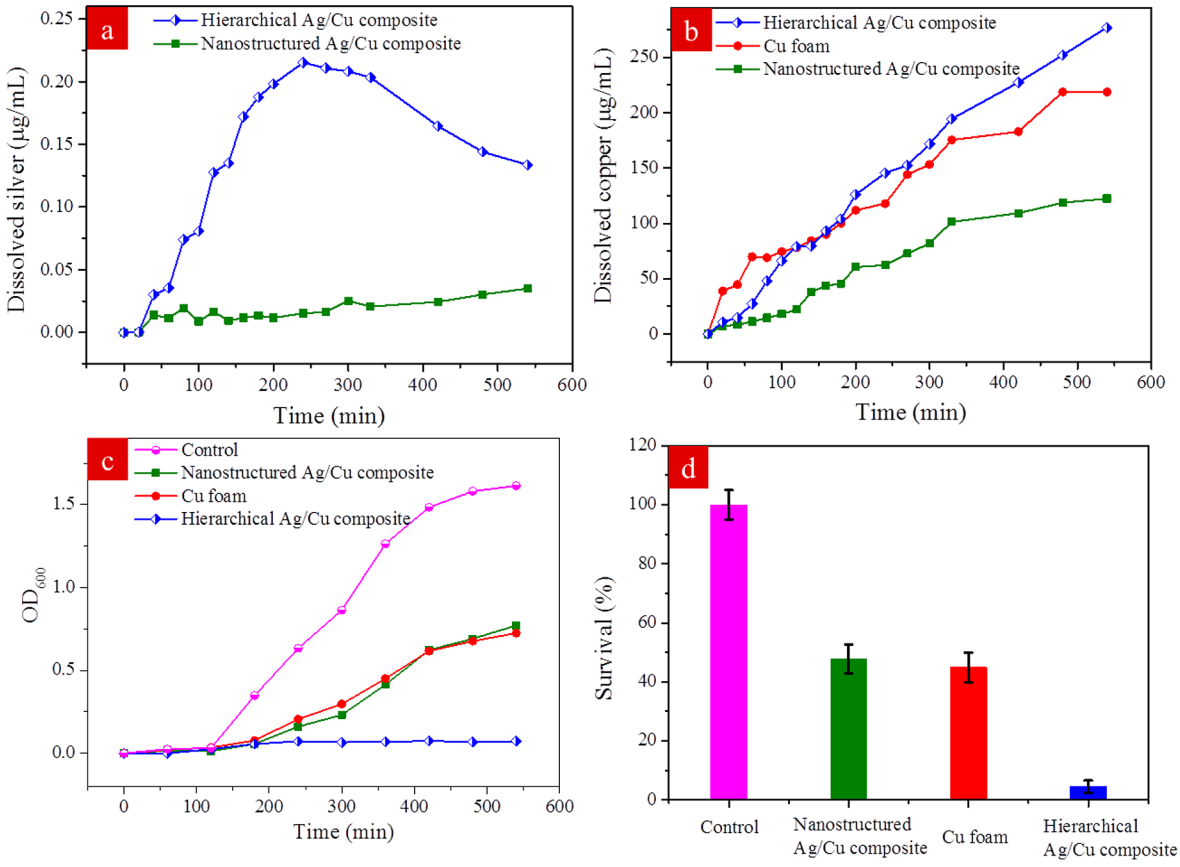

Figure 3. Antibacterial activity measurement using the turbidity assay. (a) Time-resolved silver ion concentration of bacterial suspension with the hierarchical bimetallic composite, and nanostructured bimetallic composite, respectively. (b) Time-resolved copper ion concentration of bacterial suspension with the hierarchical bimetallic composite, nanostructured bimetallic composite, and porous copper foam, respectively. (c) Optical density (OD) measurements (at 600 nm) showing the distinctively different growth of bacteria in suspensions with different samples. (d) Comparison of the survival rate of bacteria in different solutions. The error bar is based on the average of three measurements.

hydrochloric acid (HCl) to remove the surface oxide layer. After rinsing with abundant water, the copper substrate was immersed into 3 mM $AgNO_3$ aqueous solution for 1 h at room temperature (eq 1). The deposition of silver nanostructure onto the copper substrate can be described using the following galvanic replacement reaction.

$$Cu + 2Ag^+ \rightarrow 2Ag + Cu^{2+} \quad (1)$$

Finally, the as-fabricated surface was heated at 150 °C for 2 h in the atmosphere to induce the metal oxides for a low surface energy.

Characterization. The morphology and chemical compositions of the as-fabricated surfaces were characterized by Environmental Scanning Electron Microscope (ESEM, FEI/Philips XL30 ESEM-FEG) with energy-dispersive spectrometry (EDS). The chemical state of the element on the surface was analyzed by X-ray Photoelectron Spectrometer (XPS, PHI5802). The static contact angle measurements were carried out by using a Digidrop (500-F1, Ramé-hart) at the room temperature. The adhesion of bacteria on the substrate was characterized by laser confocal scanning microscope (Leica, SPE). Concentrations of copper and silver ions were quantified by Inductively Coupled Plasma Atomic Emission Spectrometer (ICP-AES).

Antibacterial Tests. The antibacterial activities of various samples were measured using the turbidity assay and the modified Kirby–Bauer method. The initial concentration of the *Staphylococcus aureus* suspension was ~10^5–10^6 CFU/mL. The bacterial suspensions with different samples were incubated in a shaking incubator at 200 rpm and 37 °C. In the turbidity assay, the optical density (OD) of the bacterial suspensions at 600 (OD_{600}) nm was measured for 9 h with a time interval of 1 h. The bacterial survival rates of various solutions, or the normalized OD values relative to that of the pure medium, were calculated. The time-resolved ion concentrations of both silver and copper were also measured with a time interval of 1 h. The growth rate and concentration of bacteria were determined by the values of OD. In the latter method, the radius of the inhibition zone was used to quantify the antibacterial activity. Briefly, a suspension of 100 μL was spread on LB-Agar plates, and then different samples were placed on top of the LB-Agar plates. After incubation at 37 °C for 24 h, the sizes of the inhibition zone of different samples were measured using the optical microscopy.

3. RESULTS AND DISCUSSION

Previously, we developed the most superhydrophobic surface ever reported, which can significantly reduce the classical contact time limit of droplets impinging on surfaces.[50] The superhydrophobic surface with a hierarchical architecture was fabricated on the porous copper foam by using a chemical etching. Distinct from our previous work, the superhydrophobic surface developed here is multiscale in surface roughness and also has bimetallic composition enabled by a facile galvanic replacement (GR) reaction.[51] The average pore diameter of the copper foam substrate we used is ~150 μm, and the width of ridges connecting the pores is ~50 μm. In our experiment, the copper foam was first washed with ethanol, 1 M hydrochloric acid (HCl), and deionized (DI) water. Then, the copper foam was immersed into a solution of 3 mM $AgNO_3$ for 60 min for the GR reaction, followed by heating at 150 °C for 2 h in the atmosphere. Figure1a shows the typical scanning electron microscope (SEM) image of the as-prepared surface. It is

apparent that the originally porous copper foam with microstructure alone is transformed into a composite with two-tier roughness. The copper pores and ridges are covered by silver dendrites with a length of 8.0 ± 0.8 μm and width of 2.5 ± 0.7 μm (Figure 1a). High-resolution image shows that the dendrites are composed of numerous nanoparticles ∼100 nm in diameter (Figure 1b). As a comparison, we also prepared the bimetallic composite with nanostructure alone based on the flat copper foil substrate using the same GR reaction process discussed above. As shown in Figure 1c,d, different from the dense silver dendrite structures obtained from the porous copper foam, the nanostructures obtained from the flat copper foil are sparse and in a coral-like shape due to the smaller nucleation sites. The nanostructures have an average length of 4.0 ± 1 0.0 μm and width of 0.8 ± 0.2 μm.

Figure 2a plots the X-ray photoelectron spectroscopy (XPS) spectra of the as-fabricated hierarchical bimetallic composite. The characteristic peaks at 530.5 (O 1s) and 974.8 eV (O KLL) result from the dissolved oxygen or the thermal oxidation of copper and silver in the heating stage. Figure 2b,c shows the high-resolution spectra of both Cu 2p and Ag 3d, respectively. The characteristic peaks at 934.4 eV (Cu $2p_{3/2}$) and 954.0 eV (Cu $2p_{5/2}$) correspond to CuO, while the binding energy of 932.0 eV (Cu $2p_{3/2}$) and 952.1 eV (Cu $2p_{1/2}$) are associated with Cu_2O.[52] Similarly, two characteristic peaks located at ∼367.8 eV (Ag $3d_{5/2}$) and 373.9 eV (Ag $3d_{3/2}$) are assigned to Ag_2O.[53] The existence of Ag_2O, Cu_2O, and CuO is further confirmed by the O 1s spectrum measurement as shown in Figure 2d.[54]

The apparent contact angle of DI water with a bacterial concentration of $\sim10^5-10^6$ CFU/mL on the hierarchical bimetallic composite is 158.6° (inset of Figure 1a). As a comparison, without the presence of the metal oxide layer, the surface is hydrophilic, revealing the effect of the metal oxide layer on the transformation of the surface wettability. Moreover, the use of the simple thermal oxidation process avoids the need for additional chemical modification step used in the fabrication of conventional superhydrophobic surfaces. The contact angle of DI water with a bacterial concentration of $\sim10^5-10^6$ CFU/mL on the nanostructured bimetallic composite is 111.2° (inset of Figure 1c). Such a smaller contact angle is due to the absence of microscale roughness as well as the smaller density of silver dendrites. To characterize the bacterial (S. aureus) adhesion on different surfaces in the dry environment, we prepared the bacterial suspension in DI water with a concentration of $\sim10^5-10^6$ CFU/mL. Then, a bacterial suspension of 10 μL was dispensed on samples. After 20 min of incubation, samples were then treated with 4% paraformaldehyde and propidium iodide (PI), respectively. Following a thorough rinsing with phosphate buffer solution (PBS) buffer, we quantified bacteria adhered to each sample using the laser scanning confocal microscope. There is no visible bacteria colony observed on the hierarchical bimetallic composite, owing to the minimal interaction between bacteria and underlying superhydrophobic substrate. By contrast, the bacterial suspension can easily penetrate into the nanostructured bimetallic composite due to its small contact angle.

To illustrate the utility of hierarchical architecture and bimetallic composition for enhanced antibacterial activity in the wet condition, we measured the time-resolved concentration of silver ion in the bacterial suspension. For the bacterial suspension consisting of the hierarchical bimetallic composite, there is a continuous increase in the silver ion concentration until it reaches a maximum silver ion concentration at ∼240 min as shown in Figure 3a. Note that although the hierarchical bimetallic surface is superhydrophobic at the beginning, its nonwetting property is gradually deteriorated due to the dissolution of the metal oxide over time.[55] Accordingly, the interaction area between the medium and underlying solid surface is dramatically enhanced. Moreover, because of the higher solubility of metal oxide (Ag_2O) than zerovalent silver in water, the release of silver ion is accelerated. Without the presence of the metal oxide, the release of silver ion in water is mainly governed by the slow oxidation of the zerovalent metallic phase by the dissolved oxygen (eqs 2 and 3).[47,56] Thus, the presence of the metal oxide coating on the hierarchical bimetallic surface not only leads to an antifouling property in the dry condition but also promotes the silver ion release in the wet condition. The reduced silver ion release after ∼240 min might be due to the depletion of metal oxides. Still, during the whole process, the release of the silver ion in the bacterial suspension with the nanostructured bimetallic surface is always slower than that in the bacterial suspension with the hierarchical bimetallic surface due to its small surface area of silver nanostructures. For example, the maximum silver concentration in the suspension with the hierarchical surface is ∼600% larger than in the bacterial suspension with the nanostructured bimetallic surface. Moreover, the released silver ion is susceptible to unwanted reaction with the Cl^-, leading to the formation of the silver precipitation, further limiting the lifetime of silver based antibacterials.[57−59]

$$4Ag(0) + O_2 \rightarrow 2Ag_2O \quad (2)$$

$$2Ag_2O + 4H^+ \rightarrow 4Ag^+ + 2H_2O \quad (3)$$

Figure 3b plots the time-resolved copper ion concentration obtained from various bacterial suspensions. Although the copper ion concentration in the suspension with the hierarchical bimetallic composite is smaller than that in the copper foam in the first 2 h, after that there is a steep increase resulting from the increasing copper area as well as the metal oxide-assisted ion release after the breakdown of the superhydrophobic property.[37,40] The maximum copper ion concentration of the suspension with the hierarchical bimetallic composite at 9 h is 277.22 μg/mL, which is 27% larger than that of the solution with the Cu foam (218.9 μg/mL) or 226% larger than that from the solution with the nanostructured bimetallic composite. Notably, the presence of the copper component in the bimetallic composite hinders the precipitation problem encountered in the silver ion release. This is confirmed by the copper ions measurements in different suspensions as shown in Figure 3b, in which we did not observe the decrease in the copper ion in the measurement up to 600 min. This is because during the whole process, the copper ion alternates between the redox states (Cu^{2+} and Cu^+) due to the interaction with the proteins in the bacterial membrane and dissolved oxygen.[60] Thus, compared to the surface with single composition or simple topography, the use of bimetallic composition in our surface can engender a sustained ion supply.

To examine the antibacterial activities of different samples, we first studied the growth of bacteria in a pure medium using the turbidity assay.[61,62] The concentration of the bacterial suspension is $\sim10^6-10^7$ CFU/mL. In the control experiment, the bacteria exhibit a time-dependent growth. As indicated by the optical density (OD) measurement at 600 nm, the bacteria keep a fast growth after 120 min, though there is no

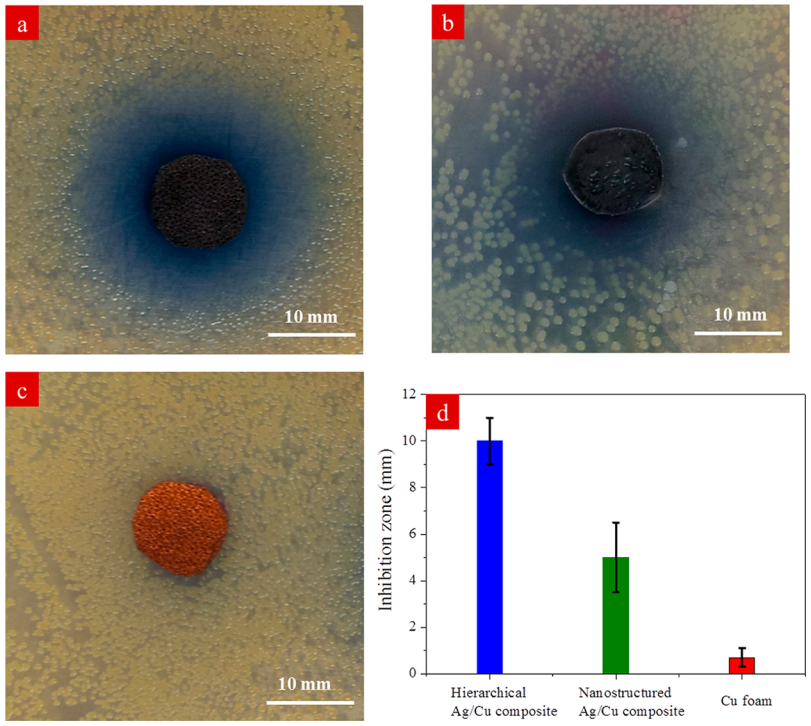

Figure 4. Antibacterial activity measurement using the modified Kirby–Bauer method. (a–c) Optical images of bacterial colonies around (a) the hierarchical bimetallic composite, (b) the nanostructured bimetallic composite, and (c) the copper foam against *S. aureus*, respectively. (d) Comparisons of the size of the inhibition zone of bacteria treated with different samples. The radius of the inhibition zone of bacteria against the hierarchical bimetallic composite is ~10 mm, which is much larger than these on the bimetallic composite with nanoscale roughness alone (~5 mm) and the copper foam (~0.7 mm). Error bar is based on the average of three measurements.

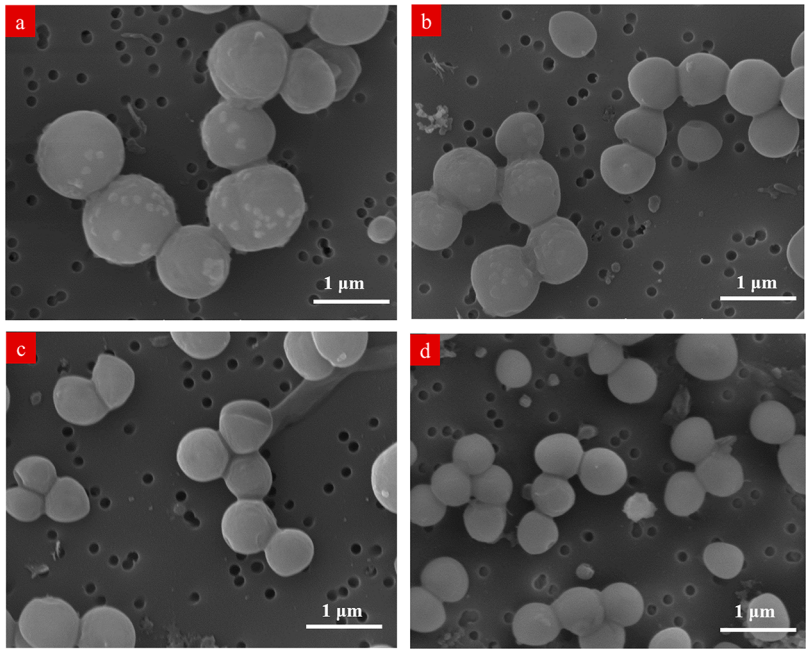

Figure 5. Bacterial morphological analysis. The average diameters of bacteria incubated in the medium with (a) the hierarchical bimetallic composite, (b) the nanostructured bimetallic composite, (c) the copper foam, and (d) the pure medium are ~900, 700, 640, and 600 nm, respectively. Moreover, the peripheral cell walls of *S. aureus* treated with the hierarchical bimetallic composite are surrounded by small granules with a diameter of ~90 ± 10 nm. By contrast, there is no granule observed on the surfaces of bacteria incubated in the suspension with the copper foam or the pure medium.

pronounced bacteria growth at the beginning (Figure 3c). After an incubation of 9 h, the suspension becomes cloudier, and the OD value increases to 1.614. By contrast, for the suspension containing the hierarchical bimetallic composite, the OD value during the whole incubation is small, and the maximum OD value is ~0.073. This OD value is 1 order of magnitude smaller

than that of the suspension with the nanostructured bimetallic composite or the copper foam. It is important to note that although the copper ion concentration in the bacterial suspension with the nanostructured bimetallic composite is far less than that in the copper foam, these two surfaces exhibit comparable antibacterial activities, confirming the synergistic cooperation of silver and copper components for enhanced antibacterial activity. To quantify the antibacterial activity, we converted the OD values measured in different solutions to the bacterial survival rate. Here, the bacterial survival rate is defined as the normalized OD value in the bacterial suspension with samples relative to that of the pure medium.[63] Figure 3d plots the survival rate of *S. aureus* in different solutions after an incubation of 9 h. The survival rate of bacteria treated by the hierarchical bimetallic composite is 4.5%, which is 1 order of magnitude lower than that of the nanostructured bimetallic composite or the copper foam, confirming that the hierarchical composite is a more effective inhibitor for bacterial growth than its counterparts that either have single-phase chemical composition (copper foam) or one-tier architecture (nanostructured bimetallic composite).

The antibacterial activities obtained on various samples are consistent with the measurement using the modified Kirby–Bauer method,[64] in which we used the radius of inhibition zone to quantify the antibacterial activity. The inhibition zone is a region where no growth of bacteria colonies was found around the sample during the testing. Briefly, in our experiment, 100 μL of *S. aureus* bacterial suspension with a concentration of $\sim 10^5-10^6$ CFU/mL was dispensed on a LB agar plate. After gently placing the samples on this LB agar plate and incubating for 24 h at 37 °C, we measured the radius of the inhibition zone. As shown in Figure 4a, the radius of the inhibition zone corresponding to the hierarchical bimetallic composite is ~10 mm, which is much larger than these on the bimetallic composite with nanoscale roughness alone (~5 mm, Figure 4b) and the copper foam (~0.7 mm, Figure 4c). Such observations suggest that the hierarchical bimetallic composite is a more effective inhibitor for the bacterial growth than its counterparts, that is, the copper foam with a single chemical composition or the nanostructured bimetallic composite with one-tier roughness alone. Note that after the release of ions in the wet condition, the hierarchical bimetallic Ag/Cu composite still maintains a good antibacterial activity, although the surface becomes superhydrophilic.

We also examined the morphologies of bacteria incubated in various suspensions with SEM. As shown in Figure 5a, after an incubation of 9 h, the surfaces of *S. aureus* in the suspension consisting of the hierarchical bimetallic composite are rough and covered by tiny granules[65] with a diameter of ~90.0 ± 10.0 nm. Note that these randomly distributed granules are also observed on the surfaces of bacteria incubated in the medium consisting of the nanostructured bimetallic composite (Figure 5b), although the amount of these granules is less than that on the bacteria incubated with the hierarchical bimetallic composite. By contrast, the surfaces of bacteria in the medium with the porous copper (Figure 5c) and the pure medium (Figure 5d) are smooth and intact, and there is no granule observed on the bacteria surfaces. Moreover, as shown in Figure 6, compared to the energy-dispersive X-ray spectroscopy (EDS) spectrum of the bacteria incubated in the pure medium, bacteria incubated in the medium with the hierarchical bimetallic composite exhibit a characteristic peak, which is assigned to the silver on the granules.[66] The presence of silver

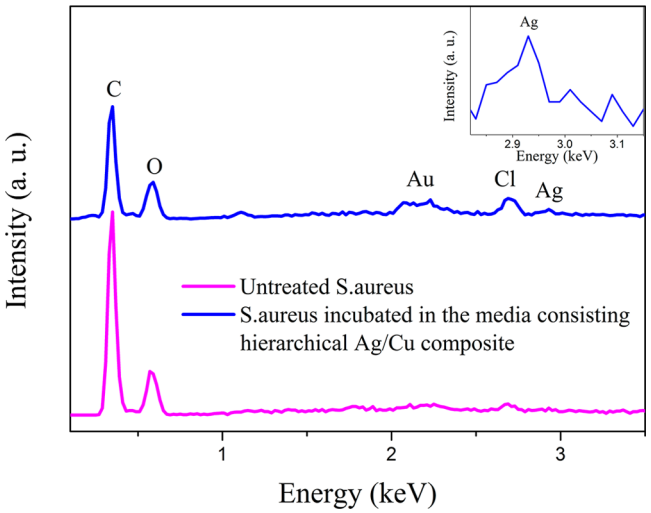

Figure 6. EDS spectra of *S. aureus* incubated in different conditions. The blue curve corresponds to the bacteria incubated in the medium with the hierarchical Ag/Cu composite, and the pink curve corresponds to the untreated bacteria. (inset) The EDS characteristic peak assigned to the silver element, suggesting the existence of silver in the granules. The absence of copper element in the granules in the EDS analysis is also consistent with our previous analysis on the copper ion, which alternates between the redox states (Cu^{2+} and Cu^{+}) during the release process.

in the granules is ascribed to the specific binding of silver ion to the negatively charged bacteria cellular membrane/wall. The absence of copper element in the granule in the EDS analysis is also consistent with our previous analysis on the copper ion, which alternates between the redox states (Cu^{2+} and Cu^{+}) during the release process.[60]

Interestingly, we found that the bacteria size is dependent on the concentrations of both silver and copper ions (Figure 5). For example, after an incubation of 9 h, the average diameter of bacteria in the medium consisting of the hierarchical bimetallic composite is 900 nm,[67] which corresponds to the largest silver and copper ion concentrations. By contrast, the average diameters of bacteria incubated in the medium with the nanostructured bimetallic composite, the copper foam, and the pure medium are ~700, 640, and 600 nm, respectively. The increase of the size of the bacteria might be caused by the interaction of ions with the bacterial membrane, though the fundamental mechanism remains to be investigated.[68] These results further confirm the synergistic cooperation effect of combined silver and copper ions on the antibacterial activity.

4. CONCLUSIONS

In summary, we developed a facile approach to fabricate a novel antibacterial surface functioning in various conditions. The surface is multiscale in structure, bimetallic in composition. Moreover, the thermal oxides covered on the rough surface lowers the surface energy, allowing for a superhydrophobic property without the need for additional surface modification as in the case of conventional superhydrophobic surfaces. Remarkably, the superhydrophobic effect can also be collapsed in the wet solution to enable the release of biocidal agents. We demonstrate that the synergy between the large surface area, the presence of the metal oxides, as well as the bimetallic composition endows an enhanced antibacterial activity in both dry and wet conditions. By further structure optimization, we

envision that the metal ions in the water can be released in an on-demand and sustained manner, making it possible to develop robust and intelligent antibacterial materials for various applications.

AUTHOR INFORMATION

Corresponding Authors

*E-mail: zuanwang@cityu.edu.hk. (Z.W.)
*E-mail: hongysun@cityu.edu.hk. (H.S.)

Notes

The authors declare no competing financial interest.

ACKNOWLEDGMENTS

We are grateful for support from the Hong Kong University Grant Council (Nos. 125312 and 21300714), National Natural Science Foundation of China (Nos. 51276152 and 51475401), and the City University of Hong Kong under Strategic Research Grant No. 7004076 and Applied Research Grant (No. 9667091).

REFERENCES

(1) Hasan, J.; Crawford, R. J.; Ivanova, E. P. Antibacterial Surfaces: The Quest for a New Generation of Biomaterials. *Trends Biotechnol.* **2013**, *31*, 295−304.

(2) Bazaka, K.; Jacob, M. V.; Crawford, R. J.; Ivanova, E. P. Efficient Surface Modification of Biomaterial to Prevent Biofilm Formation and the Attachment of Microorganisms. *Appl. Microbiol. Biotechnol.* **2012**, *95*, 299−311.

(3) Arciola, C. R.; Campoccia, D.; Speziale, P.; Montanaro, L.; Costerton, J. W. Biofilm Formation in Staphylococcus Implant Infections. A Review of Molecular Mechanisms and Implications for Biofilm-resistant Materials. *Biomaterials* **2012**, *33*, 5967−5982.

(4) Xu, L. C.; Siedlecki, C. A. Submicron-textured Biomaterial Surface Reduces Staphylococcal Bacterial Adhesion and Biofilm Formation. *Acta Biomater.* **2012**, *8*, 72−81.

(5) Tiller, J. C.; Liao, C. J.; Lewis, K.; Klibanov, A. M. Designing Surfaces that Kill Bacteria on Contact. *Proc. Natl. Acad. Sci. U. S. A.* **2001**, *98*, 5981−5985.

(6) Levy, S. B.; Marshall, B. Antibacterial Resistance Worldwide: Causes, Challenges and Responses. *Nat. Med.* **2004**, *10*, S122−S129.

(7) Davies, D. Understanding Biofilm Resistance to Antibacterial Agents. *Nat. Rev. Drug Discovery* **2003**, *2*, 114−122.

(8) Hu, W.; Peng, C.; Luo, W.; Lv, M.; Li, X.; Li, D.; Huang, Q.; Fan, C. Graphene-Based Antibacterial Paper. *ACS Nano* **2010**, *4*, 4317−4323.

(9) Wong, T. S.; Kang, S. H.; Tang, S. K. Y.; Smythe, E. J.; Hatton, B. D.; Grinthal, A.; Aizenberg, J. Bioinspired Self-repairing Slippery Surfaces with Pressure-stable Omniphobicity. *Nature* **2011**, *477*, 443−447.

(10) Ocsoy, I.; Paret, M. L.; Ocsoy, M. A.; Kunwar, S.; Chen, T.; You, M. X.; Tan, W. H. Nanotechnology in Plant Disease Management: DNA-Directed Silver Nanoparticles on Graphene Oxide as an Antibacterial against Xanthomonas Perforans. *ACS Nano* **2013**, *7*, 8972−8980.

(11) Thiel, J.; Pakstis, L.; Buzby, S.; Raffi, M.; Ni, C.; Pochan, D. J.; Shah, S. I. Antibacterial Properties of Silver-doped Titania. *Small* **2007**, *3*, 799−803.

(12) Liu, J. Y.; Sonshine, D. A.; Shervani, S.; Hurt, R. H. Controlled Release of Biologically Active Silver from Nanosilver Surfaces. *ACS Nano* **2010**, *4*, 6903−6913.

(13) AshaRani, P. V.; Mun, G. L. K.; Hande, M. P.; Valiyaveettil, S. Cytotoxicity and Genotoxicity of Silver Nanoparticles in Human Cells. *ACS Nano* **2009**, *3*, 279−290.

(14) Li, Y.; Zhang, W.; Niu, J. F.; Chen, Y. S. Mechanism of Photogenerated Reactive Oxygen Species and Correlation with the Antibacterial Properties of Engineered Metal-Oxide Nanoparticles. *ACS Nano* **2012**, *6*, 5164−5173.

(15) Carlson, C.; Hussain, S. M.; Schrand, A. M.; Braydich-Stolle, L. K.; Hess, K. L.; Jones, R. L.; Schlager, J. J. Unique Cellular Interaction of Silver Nanoparticles: Size-Dependent Generation of Reactive Oxygen Species. *J. Phys. Chem. B* **2008**, *112*, 13608−13619.

(16) Feng, Q. L.; Wu, J.; Chen, G. Q.; Cui, F. Z.; Kim, T. N.; Kim, J. O. A Mechanistic Study of the Antibacterial Effect of Silver Ions on Escherichia coli and Staphylococcus aureus. *J. Biomed. Mater. Res.* **2000**, *52*, 662−668.

(17) Morones-Ramirez, J. R.; Winkler, J. A.; Spina, C. S.; Collins, J. J. Silver Enhances Antibiotic Activity Against Gram-negative Bacteria. *Sci. Transl. Med.* **2013**, *5*, 190−81.

(18) Besinis, A.; De Peralta, T.; Handy, R. D. Inhibition of Biofilm Formation and Antibacterial Properties of a Silver Nano-coating on Human Dentine. *Nanotoxicology* **2014**, *8*, 745−754.

(19) Lin, W. T.; Tan, H. L.; Duan, Z. L.; Yue, B.; Ma, R.; He, G.; Tang, T. T. Inhibited Bacterial Biofilm Formation and Improved Osteogenic Activity on Gentamicin-loaded Titania Nanotubes with Various Diameters. *Int. J. Nanomed.* **2014**, *9*, 1213−1228.

(20) Rizzello, L.; Sorce, B.; Sabella, S.; Vecchio, G.; Galeone, A.; Brunetti, V.; Cingolani, R.; Pompa, P. P. Impact of Nanoscale Topography on Genomics and Proteomics of Adherent Bacteria. *ACS Nano* **2011**, *5*, 1865−1876.

(21) Koch, K.; Bhushan, B.; Jung, Y. C.; Barthlott, W. Fabrication of Artificial Lotus Leaves and Significance of Hierarchical Structure for Superhydrophobicity and Low Adhesion. *Soft Matter* **2009**, *5*, 1386−1393.

(22) Liu, K.; Jiang, L. Bio-inspired Self-cleaning Surfaces. *Annu. Rev. Mater. Res.* **2012**, *42*, 231−263.

(23) Bixler, G. D.; Bhushan, B. Bioinspired Rice Leaf and Butterfly Wing Surface Structures Combining shark Skin and Lotus Effects. *Soft Matter* **2012**, *8*, 11271−11284.

(24) Nosonovsky, M.; Bhushan, B. Superhydrophobic Surfaces and Emerging Applications: Non-adhesion, Energy, Green Engineering. *Curr. Opin. Colloid Interface Sci.* **2009**, *14*, 270−280.

(25) Zheng, Y.; Bai, H.; Huang, Z.; Tian, X.; Nie, F. Q.; Zhao, Y.; Zhai, J.; Jiang, L. Directional Water Collection on Wetted Spider Silk. *Nature* **2010**, *463*, 640−643.

(26) Erbil, H.; Demirel, A. L.; Avci, Y.; Mert, O. Transformation of a Simple Plastic into a Superhydrophobic Surface. *Science* **2003**, *299*, 1377−1380.

(27) Chen, X. M.; Wu, J.; Ma, R. Y.; Hua, M.; Koratkar, N.; Yao, S. H.; Wang, Z. K. Nanograssed Micropyramidal Architectures for Continuous Dropwise Condensation. *Adv. Funct. Mater.* **2011**, *21*, 4617−4623.

(28) Zhang, X.; Shi, F.; Niu, J.; Jiang, Y. G.; Wang, Z. Q. Superhydrophobic Surfaces: From Structural Control to Functional Application. *J. Mater. Chem.* **2008**, *18*, 621−633.

(29) Lau, K. K. S.; Bico, J.; Teo, K. B. K.; Chhowalla, M.; Amaratunga, G. A. J.; Milne, W. I.; McKinley, G. H.; Gleason, K. K. Superhydrophobic Carbon Nanotube Forests. *Nano Lett.* **2003**, *3*, 1701−1705.

(30) Tuteja, A.; Choi, W.; Ma, M. L.; Mabry, J. M.; Mazzella, S. A.; Rutledge, G. C.; McKinley, G. H.; Cohen, R. E. Designing Superoleophobic Surfaces. *Science* **2007**, *318*, 1618−1622.

(31) Lafuma, A.; Quere, D. Superhydrophobic States. *Nat. Mater.* **2003**, *2*, 457−460.

(32) Zhang, X.; Wang, L.; Levanen, E. Superhydrophobic Surfaces for the Reduction of Bacterial Adhesion. *RSC Adv.* **2013**, *3*, 12003−12020.

(33) Zhang, L.; Zhang, Z.; Wang, P. Smart Surfaces with Switchable Superoleophilicity and Superoleophobicity in Aqueous Media: Toward Controllable Oil/Water Separation. *NPG Asia Mater.* **2012**, *4*, e8.

(34) Privett, B. J.; Youn, J.; Hong, S. A.; Lee, J.; Han, J.; Shin, J. H.; Schoenfisch, M. H. Antibacterial Fluorinated Silica Colloid Superhydrophobic Surfaces. *Langmuir* **2011**, *27*, 9597−9601.

(35) Wood, T. J.; Hurst, G. A.; Schofield, W. C. E.; Thompson, R. L.; Oswald, G.; Evans, J. S. O.; Sharples, G. J.; Pearson, C.; Petty, M. C.; Badyal, J. P. S. Electroless Deposition of Multi-Functional Zinc Oxide

Surfaces Displaying Photoconductive, Superhydrophobic, Photowetting, and Antibacterial Properties. *J. Mater. Chem.* **2012**, *22*, 3859−3867.
(36) Khalil-Abad, M. S.; Yazdanshenas, M. E. Superhydrophobic Antibacterial Cotton Textiles. *J. Colloid Interface Sci.* **2010**, *351*, 293−298.
(37) Papadopoulos, P.; Mammen, L.; Deng, X.; Vollmer, D.; Butt, H. J. How Superhydrophobicity Breaks Down. *Proc. Natl. Acad. Sci. U. S. A.* **2013**, *110*, 3254−3258.
(38) Friedlander, R. S.; Vlamakis, H.; Kim, P.; Khan, M.; Kolter, R.; Aizenberg, J. Bacterial Flagella Explore Microscale Hummocks and Hollows to Increase Adhesion. *Proc. Natl. Acad. Sci. U. S. A.* **2013**, *110*, 5624−5629.
(39) Patankar, N. A. Transition between Superhydrophobic States on Rough Surfaces. *Langmuir* **2004**, *20*, 7097−7102.
(40) Kusumaatmaja, H.; Blow, M. L.; Dupuis, A.; Yeomans, J. M. The Collapse Transition on Superhydrophobic Surfaces. *Europhys. Lett.* **2008**, *81*, 36003.
(41) Goodman, A. M.; Cao, Y.; Urban, C.; Neumann, O.; Ayala-Orozco, C.; Knight, M. W.; Joshi, A.; Nordlander, P.; Halas, N. J. The Surprising in Vivo Instability of Near-IR-Absorbing Hollow Au-Ag Nanoshells. *ACS Nano* **2014**, *8*, 3222−3231.
(42) Zhang, H.; Jin, M. S.; Wang, J. G.; Li, W. Y.; Camargo, P. H. C.; Kim, M. J.; Yang, D. R.; Xie, Z. X.; Xia, Y. N. Synthesis of Pd-Pt Bimetallic Nanocrystals with a Concave Structure through a Bromide-Induced Galvanic Replacement Reaction. *J. Am. Chem. Soc.* **2011**, *133*, 6078−6089.
(43) Gu, C. D.; Ren, H.; Tu, J. P.; Zhang, T. Y. Micro/Nanobinary Structure of Silver Films on Copper Alloys with Stable Water-Repellent Property under Dynamic Conditions. *Langmuir* **2009**, *25*, 12299−12307.
(44) Liu, R.; Sen, A. Unified Synthetic Approach to Silver Nanostructures by Galvanic Displacement Reaction on Copper: From Nanobelts to Nanoshells. *Chem. Mater.* **2012**, *24*, 48−54.
(45) Liu, J. Y.; Hurt, R. H. Ion Release Kinetics and Particle Persistence in Aqueous Nano-Silver Colloids. *Environ. Sci. Technol.* **2010**, *44*, 2169−2175.
(46) Xiu, Z. M.; Ma, J.; Alvarez, P. J. J. Differential Effect of Common Ligands and Molecular Oxygen on Antimicrobial Activity of Silver Nanoparticles versus Silver Ions. *Environ. Sci. Technol.* **2011**, *45*, 9003−9008.
(47) Jones, A. M.; Garg, S.; He, D.; Pham, A. N.; Waite, T. D. Superoxide-Mediated Formation and Charging of Silver Nanoparticles. *Environ. Sci. Technol.* **2011**, *45*, 1428−1434.
(48) Grillet, N.; Manchon, D.; Cottancin, E.; Bertorelle, F.; Bonnet, C.; Broyer, M.; Lermé, J.; Pellarin, M. Photo-Oxidation of Individual Silver Nanoparticles: A Real-Time Tracking of Optical and Morphological Changes. *J. Phys. Chem. C* **2013**, *117*, 2274−2282.
(49) Lok, C. N.; Ho, C. M.; Chen, R.; He, Q. Y.; Yu, W. Y.; Sun, H.; Tam, P. K. H.; Chiu, J. F.; Che, C. M. Silver Nanoparticles: Partial Oxidation and Antibacterial Activities. *J. Biol. Inorg. Chem.* **2007**, *12*, 527−534.
(50) Liu, Y.; Moevius, L.; Xu, X.; Qian, T.; Yeomans, J. M.; Wang, Z. Pancake Bouncing on Superhydrophobic Surfaces. *Nat. Phys.* **2014**, *10*, 515−519.
(51) Banerjee, M.; Sharma, S.; Chattopadhyay, A.; Ghosh, S. S. Enhanced Antibacterial Activity of Bimetallic Gold-silver Core-shell Nanoparticles at Low Silver Concentration. *Nanoscale* **2011**, *3*, 5120−5125.
(52) Zhang, Z. H.; Wang, P. Highly Stable Copper Oxide Composite as an Effective Photocathode for Water Splitting via a Facile Electrochemical Synthesis Strategy. *J. Mater. Chem.* **2012**, *22*, 2456−2464.
(53) Wang, D.; Zhou, Z. H.; Yang, H.; Shen, K. B.; Huang, Y.; Shen, S. Preparation of TiO_2 Loaded with Crystalline Nano Ag by a One-step Low-temperature Hydrothermal Method. *J. Mater. Chem.* **2012**, *22*, 16306−16311.
(54) Han, Y.; Lupitskyy, R.; Chou, T. M.; Stafford, C. M.; Du, H.; Sukhishvili, S. Effect of Oxidation on Surface-Enhanced Raman Scattering Activity of Silver Nanoparticles: A Quantitative Correlation. *Anal. Chem.* **2011**, *83*, 5873−5880.
(55) Xiu, Z. M.; Zhang, Q. B.; Puppala, H. L.; Colvin, V. L.; Alvarez, P. J. J. Negligible Particle-Specific Antibacterial Activity of Silver Nanoparticles. *Nano Lett.* **2012**, *12*, 4271−4275.
(56) Glover, R. D.; Miller, J. M.; Hutchison, J. E. Generation of Metal Nanoparticles from Silver and Copper Objects: Nanoparticle Dynamics on Surfaces and Potential Sources of Nanoparticles in the Environment. *ACS Nano* **2011**, *5*, 8950−8957.
(57) Ratte, H. T. Bioaccumulation and Toxicity of Silver Compounds: A Review. *Environ. Toxicol. Chem.* **1999**, *18*, 89−108.
(58) Choi, O.; Cleuenger, T. E.; Deng, B. L.; Surampalli, R. Y.; Ross, L.; Hu, Z. Q. Role of Sulfide and Ligand Strength in Controlling Nanosilver Toxicity. *Water Res.* **2009**, *43*, 1879−1886.
(59) Wang, J. M.; Huang, C. P.; Pirestani, D. Interactions of Silver with Wastewater Constituents. *Water Res.* **2003**, *37*, 4444−4452.
(60) Grass, G.; Rensing, C.; Solioz, M. Metallic Copper as an Antimicrobial Surface. *Appl. Environ. Microbiol.* **2011**, *77*, 1541−1547.
(61) Lv, M.; Su, S.; He, Y.; Huang, Q.; Hu, W. B.; Li, D.; Fan, C. H.; Lee, S. T. Long-term Antimicrobial Effect of Silicon Nanowires Decorated with Silver Nanoparticles. *Adv. Mater.* **2010**, *22*, 5463−5467.
(62) Song, J.; Kang, H.; Lee, C.; Hwang, S. H.; Jang, J. Aqueous Synthesis of Silver Nanoparticle Embedded Cationic Polymer Nanofibers and Their Antibacterial Activity. *ACS Appl. Mater. Interfaces* **2012**, *4*, 460−465.
(63) Bai, H. W.; Liu, Z. Y.; Sun, D. D. Hierarchical ZnO/Cu ″Corn-like″ Materials with High Photodegradation and Antibacterial Capability under Visible Light. *Phys. Chem. Chem. Phys.* **2011**, *13*, 6205−6210.
(64) Kong, H.; Jang, J. Antibacterial Properties of Novel Poly(methyl methacrylate) Nanofiber Containing Silver Nanoparticles. *Langmuir* **2008**, *24*, 2051−2056.
(65) Ivask, A.; ElBadawy, A.; Kaweeteerawat, C.; Boren, D.; Fischer, H.; Ji, Z. X.; Chang, C. H.; Liu, R.; Tolaymat, T.; Telesca, D.; Zink, J. I.; Cohen, Y.; Holden, P. A.; Godwin, H. A. Toxicity Mechanisms in Escherichia coli Vary for Silver Nanoparticles and Differ from Ionic Silver. *ACS Nano* **2014**, *8*, 374−386.
(66) Morones, J. R.; Elechiguerra, J. L.; Camacho, A.; Holt, K.; Kouri, J. B.; Ramirez, J. T.; Yacaman, M. J. The Bactericidal Effect of Silver Nanoparticles. *Nanotechnology* **2005**, *16*, 2346−2353.
(67) Li, W. R.; Xie, X. B.; Shi, Q. S.; Zeng, H. Y.; Ou-Yang, Y. S.; Chen, Y. B. Antibacterial Activity and Mechanism of Silver Nanoparticles on Escherichia coli. *Appl. Microbiol. Biotechnol.* **2010**, *85*, 1115−1122.
(68) Jung, W. K.; Koo, H. C.; Kim, K. W.; Shin, S.; Kim, S. H.; Park, Y. H. Antibacterial Activity and Mechanism of Action of the Silver Ion in Staphylococcus aureus and Escherichia coli. *Appl. Environ. Microbiol.* **2008**, *74*, 2171−2178.